Geomechanics and Engineering, *Vol. 20, No. 6 (2020) 547-556*
DOI: https://doi.org/10.12989/gae.2020.20.6.547

The influence of magmatic rock thickness on fracture and instability law of mining surrounding rock

Yanchao Xue[1a], Wenbin Sun*[2] and Quansen Wu[3b]

[1]*School of Resources & Civil Engineering, Northeastern University, Shenyang 110819, China*
[2]*College of Mining and Safety Engineering, Shandong University of Science and Technology, Qingdao 266590, China*
[3]*Department of Chemistry and Chemical Engineering, Jining University, Qufu 273100, China*

(Received October 21, 2019, Revised February 9, 2020, Accepted February 27, 2020)

Abstract. An understanding of the influence of MR (Magmatic Rock) thickness on the surrounding rock behaviors is essential for the prevention and management of dynamic disasters in coal mining. In this study, we used FLC3D to study the breaking and instability laws of surrounding rock with different MR thicknesses in terms of strata movement, stress and energy. The mechanism of dynamic disasters was revealed. The results show that the thicker the MR is, (1) the smaller the subsidence of the overlying strata is, but the subsidence span of the overlying strata become wider, and the corresponding displacement deformation value of the basin edge become smaller. (2) the slower the growth rate of abutment pressure in front of the working face is, but the peak value is smaller, and the influence range is larger. The peak value decreases rapidly after the breaking, and the stress concentration coefficient is maintained at about 1.31. (3) the slower the peak energy in front of coal wall, but the range of energy concentration increases (isoline "O" type energy circle). Finally, a case study was conducted to verify the disaster-causing mechanism. We anticipate that the research findings presented herein can assist in the control of dynamic hazards.

Keywords: strata behaviors; dynamic hazards; numerical simulation; rock break; coal mine

1. Introduction

Magmatic intrusion exists in many coal measures strata in North China and Huaihe River Basin (Jiang *et al*. 2019, Liu *et al*. 2019, Sun *et al.* 2019a, b, Zhao *et al.* 2020). The intrusive TMRs (Thick Magmatic Rocks) have the characteristics of high strength and good integrity, so they are often referred to as HTKRS (Hard and Thick Key Rock Strata). In the process of coal seam mining, TMRs are suspended in a large area, forming high secondary stress in the surrounding rock of the stope, accumulating a large amount of elastic strain energy. Once the TMRs are broken and unstable, the impact of large load energy can easily cause strong dynamic disasters such as mine earthquakes, impact ground pressure and dynamic load of supports, which seriously threaten the safety of coal mine production (Dewandel *et al.* 2011, Konicek *et al.* 2013, Dou *et al.* 2014, Wang *et al.* 2015, Zhao *et al.* 2018, Sun and Xue 2019, Zhou *et al.* 2020a).

As the basis of research on the breaking movement of TMRs, scholars have done a lot of work in theoretical analysis of stope strata. Nawrocki (1990) simulated the roof with shear beams and obtained the stress distribution in the deformation zone of the coal seam. Qian *et al*. (1996) established Kirchhoff plate mechanics model based on Winkler elasticity under different mining conditions according to the stress environment and characteristics of overburden before and after strata fracture. Tan *et al*. (2006) regarded the mining roof strata as a rock beam structure supported by elasticity of underlying strata, coal seams and shallow floor strata. The fracture form and initial fracture location of the basic roof were analyzed by thin plate theory. Under the condition of TMR occurrence, the overburden structure of stope presents different characteristics. Jiang *et al*. (2015) studied the evolution law of fracture development and bed separation range of overburden under the occurrence condition of high HTKRS, and gave the prediction formula of bed separation development volume and area based on elastic foundation beam model. Zhang *et al*. (2017) applied physical similarity simulation experiments to study the overburden structure and its evolution characteristics during mining, and summarized the overburden failure structure when the face was covered with single-layer and double-layer HTKRS.

In recent years, an increasing number of studies have focused on the fracture of TMRs and the distribution of abutment stress in stope. MR fragments from a strain-burst event were studied under a Scanning Electron Microscope in order to interpret failure mechanism (Heal, 2010, Mazaira and Konicek 2015, Keneti and Sainsbury 2018). The evolution of double-layer TMR separation and fracture with the corresponding MS (Microseismic) signals were investigated based on in situ observations (Lu *et al.* 2016). Through the on-site SOS MS monitoring, the MR migration and breaking state were analyzed, the risk of rock burst in Haizi coal mine was evaluated, and the influence of TMRs on coal and gas outburst was discussed (Wang *et al.* 2013).

*Corresponding author, Ph.D.
E-mail: swb@sdust.edu.cn
[a]Ph.D. Student
E-mail: stxycgs@126.com
[b]Ph.D.

ISSN: 2005-307X (Print), 2092-6219 (Online)

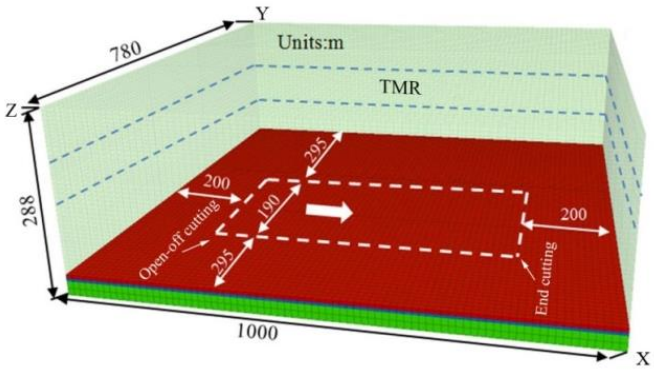

Fig. 1 FLAC3D numerical model

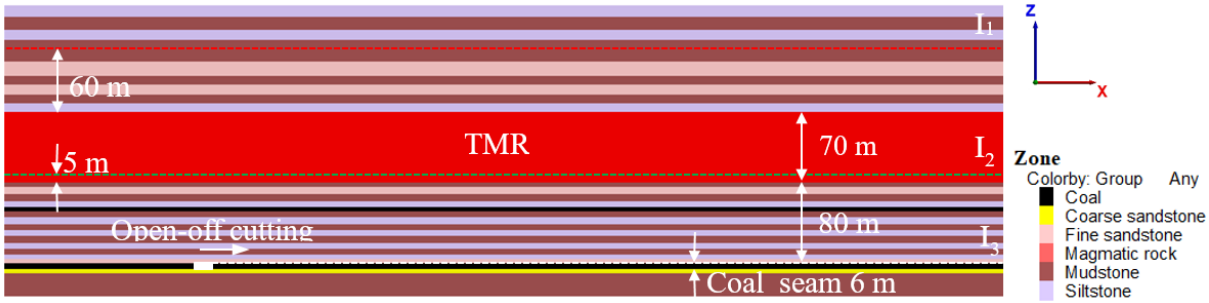

Fig. 2 Model strata and layout of monitoring lines along y=360 m

In another study, apparent-depth effects of dynamic THRS failure on the underlying coal mining were investigated based on in situ measurement results (Xu *et al.* 2019). However, few studies have considered the influence of thickness of MR on the mining surrounding rock behaviors.

Based on the previous research results, this study first analyzed the evolution law of surrounding rock movement, stress and energy when the MR thickness was 70 m and the occurrence height was 80 m, and studied the mechanism of geodynamic hazard induction using FLC3D. In order to explore the influence of MR thickness on the failure and instability of mining surrounding rock, we then compared and analyzed the evolution law of surrounding rock migration, stress and energy when the thickness of MR was 40 m, 50 m, 60 m, 70 m and 80 m at the same occurrence height, 80 m. The research findings presented herein may be of significance for the control of dynamic hazards below TMRs.

Table 1 Model strata and mechanical parameters

Lithology	Density ($kg \cdot m^{-3}$)	Bulk modulus (GPa)	Shear modulus (GPa)	Cohesion (MPa)	Tensile strength (MPa)	Friction (°)
Coal	1350	4.8	3.6	1	0.8	28
Fine sandstone	2530	12.3	8.3	3.4	3.2	35
Coarse sandstone	2530	26.4	20.7	4.3	3.8	37
Magmatic rock	3000	38.7	29.7	6.2	7.5	42
Siltstone	2530	15.2	9.4	2.8	2.4	30
Mudstone	2340	7.1	5.1	1.2	2.4	25

2. FLAC3D numerical model Description

Based on an existing TMRs mentioned in the previous section, a three-dimensional numerical calculation model of 1000 m (length) × 780 m (width) × 288 m (height) was established as shown in Fig. 1. Considering that the failure of rock is mainly shear failure, the Mohr-Coulomb model was adopted in the model analysis (Itasca 2012, Zhang 2014). The model strata and mechanical parameters are shown in Fig. 2 and Table 1. The buried depth of the simulated coal seam was 600 m and the coal seam inclination was 0°. The thickness and strength of the TMR in the model were much higher than those of other strata, which was 70 m, and distance from the coal seam was 80 m. When the thickness of MR changed, only the height of the model was changed. In order to eliminate the influence of boundary effect, 200 m and 150 m wide coal pillars were set up along the strike and inclination of the working face. In the model, the coal seam was mined for 20 m along the x-axis in each step, and the next step was carried out after balance until the TMR was broken.

The lateral displacement in X and Y directions was constrained in horizontal direction, the bottom was fully constrained, and the top was free boundary condition. The uniform compensation load applied to the top of the model was:

$$\sigma_v = \gamma h_v = 8.8 \text{ MPa} \quad (1)$$

where γ is the average bulk density of the failed simulated strata, 25.5 $kN \cdot m^{-3}$ (Herget 1987), h_v is the height of the failed simulated strata, 345 m, which was obtained by subtracting the simulated height of the overlying strata, 255 m from the depth at which the coal was being mined, 600 m As shown in Fig. 2, three displacement and stress

monitoring lines were arranged in the overburden, marked I_1- I_3, to monitor the behavior of overlying strata in different horizons.

3. Numerical simulation results and discussions

3.1 Surrounding rock fracture and instability law

3.1.1 Movement of overlying strata

Fig. 3 shows the evolution process of strata subsidence curve at 60 m above the TMR (monitoring line I_1 in Fig. 2). The subsidence of overlying strata of TMR increased uniformly with the advance of working face before the breaking, and the maximum sinking point continued to move forward, and the subsidence span increased continuously. Before the TMR was broken, the maximum subsidence of the overburden was only 0.68 m, and the maximum subsidence after breaking increased sharply to 3.06 m. The sharp fracture and subsidence of MR lost the support for the overburden and was accompanied by strong tensile stress. When the damage develops to the surface, it can cause a large subsidence basin on the surface (Swift *et al*. 2014, Tadisetty *et al.* 2006).

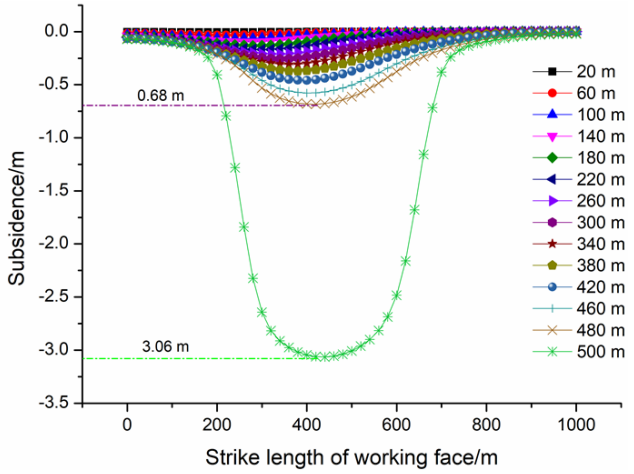

Fig. 3 Evolution of subsidence curve of overlying strata before and after the initial fracture of TMR

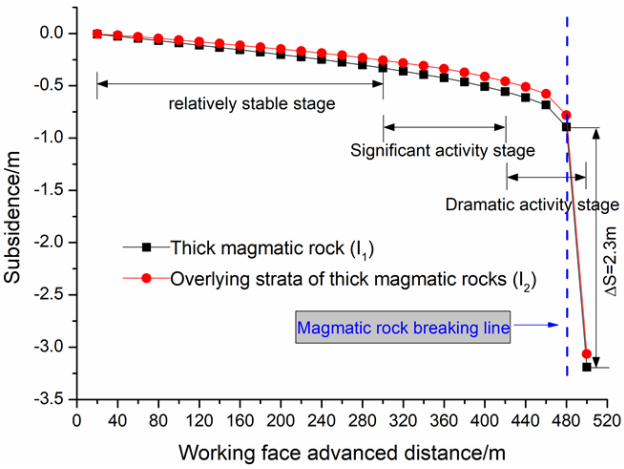

Fig. 4 Maximum subsidence of TMR and its overlaying strata with different advancing distances

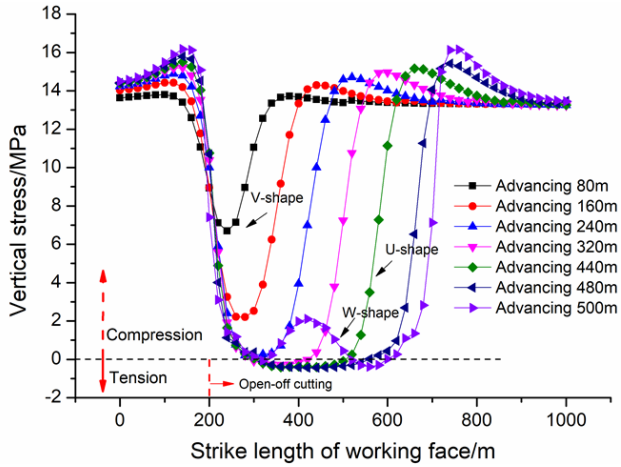

Fig. 5 Distribution characteristics of vertical stress at the bottom of TMR

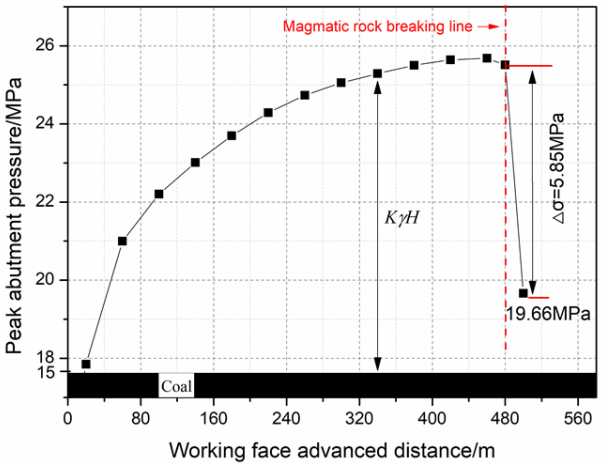

Fig. 6 Peak variation curve of front abutment pressure of working face

Fig. 4 shows the maximum subsidence curve of TMR (monitoring line I_2 in Fig. 2) and its overlying strata at different advancing distances. During the working face advancing 0-300 m, the displacement change of TMR was relatively small, and the subsidence movement of overlying strata kept pace with that of TMR, which increased linearly with the advancing of working face. The subsidence speed was 9 mm/10 m (defined as the ratio of phase subsidence increment to phase advancing distance, unit: mm/10 m), and TMR was in a relatively stable stage. The relatively stable stage of TMR lasted for a long time, which was also determined by its own characteristics.

At 300-420 m, with the periodic collapse of the coal seam roof, the bed separation fissures continued to develop upward, and the TMR began to appear more obvious bending subsidence. The maximum subsidence speed of the overlying strata increased to 19 mm/10 m, which was in a significant activity stage.

At 420-500 m, the TMR entered the stage of dramatic movement. At this time, the longitudinal tensile fracture crack (Wu *et al.* 2018) began to appear at the lower end of the middle part of the TMR. The maximum subsidence speed of the overburden during the period of 420-480 m

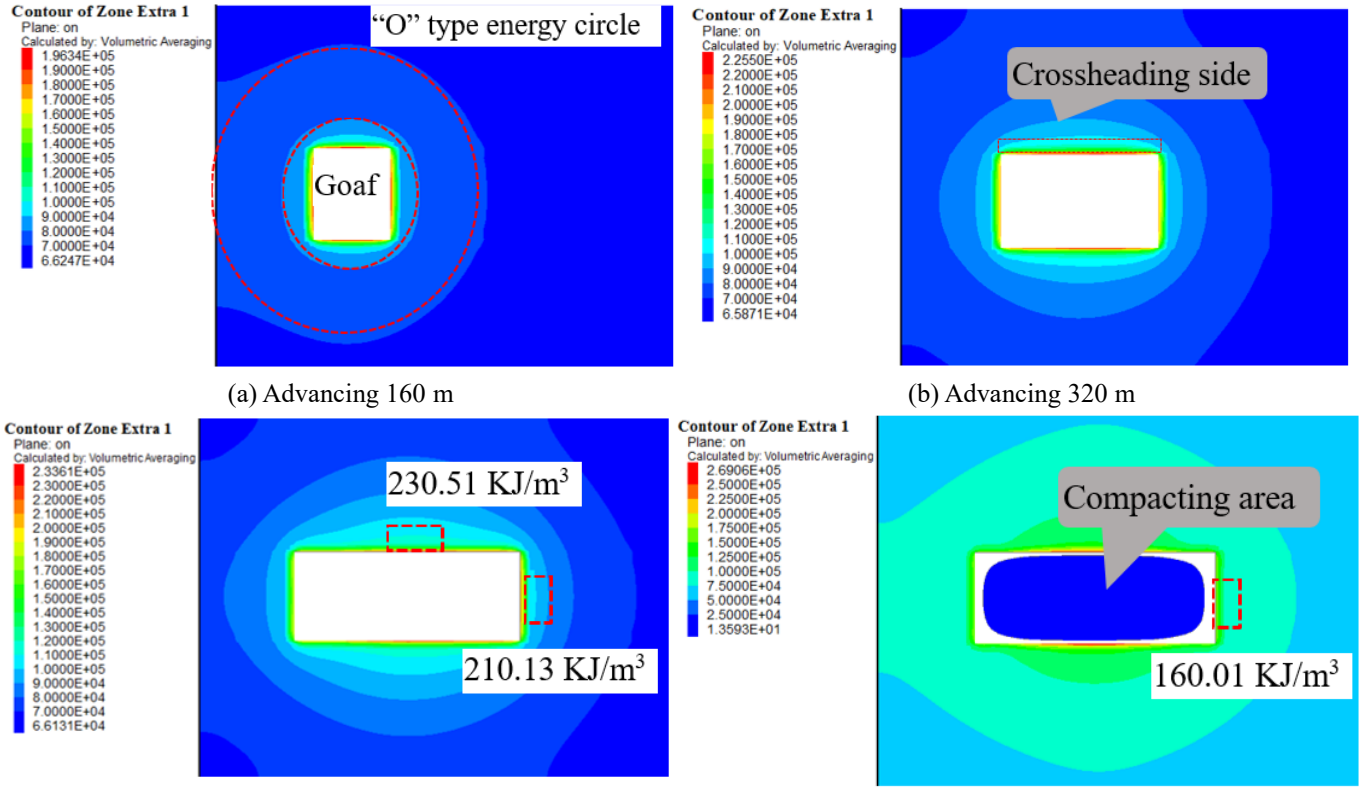

Fig. 7 Top view of elastic energy distribution in the middle of coal seam

before the fracture was 40 mm/10 m, twice the speed of the significant activity stage. When advancing to 500 m, the TMR broke for the first time, and the subsidence increased by leaps, from 0.89 m to 3.19 m. The overlying strata sank synchronously, resulting in the maximum subsidence speed of the overlying strata increased to 330 mm/10 m during the dramatic activity stage.

3.1.2 Dynamic distribution of stress

Fig. 5 shows the dynamic distribution of stress at the bottom of TMR with different advancing distances (monitoring line I_2 in Fig. 2). In a fracture cycle, the bottom of MR undergone the dynamic process of compression, tension and compression, and the vertical stress curve shape undergone the evolution from "V-shape" to "U-shape" and then to "W-shape". In the early stage of mining, the mining disturbance had little influence on it (Chen *et al*. 2019, Fu *et al.* 2020). The stress at both ends of the goaf was slightly concentrated, the bottom of MR was compressed, and the stress curve showed "V-shape". With the advance of the working face, the periodic collapse of the weak rock strata under the MR changed the stress state at the bottom, from the original compressive stress to the tensile stress, and the stress curve presented "U-shape". In this stage, the tensile stress appeared at the bottom of TMR above the middle of goaf, which indicated that the middle of TMR reached the bending strength first, and the cracking point appeared. When the vertical cracks pass through, the first bending tensile fracture occurs. At 500 m, the stress on the bottom of TMR exceeded its bending strength, and the first bending tensile fracture occurred. The broken MR block had a rapid

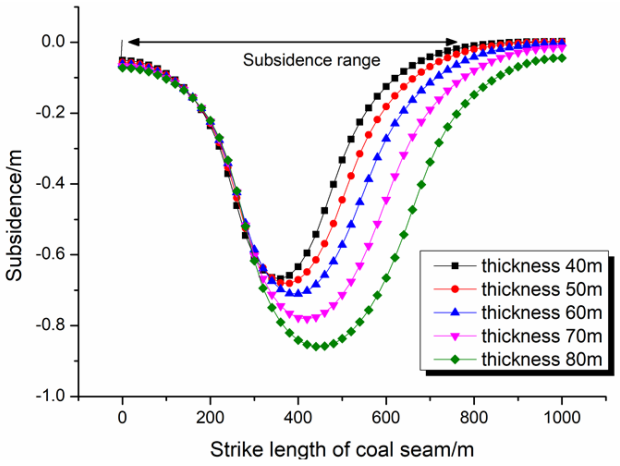

Fig. 8 Subsidence of overlying strata before the breaking of MR with different thickness

sliding and sinking movement, resulting in the underlying collapsed rock strata being basically compacted, and the bottom stress changed from tension to compression, and the stress curve presented a "W-shape".

Fig. 6 shows the variation curve of the peak front abutment pressure of working face (monitoring line I_3 in Fig. 2). In the early stage of mining, the peak value of front abutment pressure increased rapidly, and then slowed down. At 460 m, the front abutment pressure reached the maximum value, 25.68 MPa, and the stress concentration coefficient was 1.71. With the continuous advance of the working face, cracks began to appear at the bottom of TMR,

and the front abutment pressure began to decrease slightly. At 480 m, the peak value of the front abutment pressure was 25.51 MPa; At 500 m, the TMR and its overlying rock mass occurred structural collapse and instability, and the front abutment pressure of the working face decreased rapidly, the peak value decreased to 19.66 MPa, which was 5.85 MPa lower than that before the fracture, with a decrease range of 22.93%. The front abutment pressure was released and the stress concentration coefficient was about 1.31.

3.1.3 Energy distribution characteristics

Before the TMR is broken, it can be regarded as an elastic foundation beam fixed up and down. At the initial stage of mining, MR will not break or slip suddenly, but will settle slowly. At this time, the load exerted by roof on coal and rock mass can be regarded as static load (Wang *et al.* 2015, Naji *et al*. 2019, Zhou *et al*. 2020b). After MR fracture, the mechanical equilibrium condition of the system is destroyed. The static load of roof is changed to dynamic load, which releases the stored elastic energy and acts on the damaged coal and rock mass.

After coal mining, isoline "O" type energy distribution circle was formed in coal and rock mass, and the more close to the goaf, the more elastic energy accumulated (see Fig. 7(a)). The energy concentration degree of both sides of the goaf was greater than that of the front and back of the working face, and the energy concentration degree was obvious along the crossheading. In the mining of the follow-up working face, the small energy MS event was easy to be induced in the crossheading along the goaf.

Before fracture, with the advance of working face, the energy range of "O" type gradually became larger, and the energy continued to increase. At 160 m, the energy value in front of the working face was 184.21 KJ/m^3, and the energy value along the crossheading was 192.56 KJ/m^3; at 480 m, the energy value reached the maximum value before breaking, 210.13 KJ/m^3 in front of the working face, and 230.51 KJ/m^3 along the crossheading.

At 500 m, the TMR broke, there was still a "O" type energy distribution circle around the goaf after fracture, but the energy value was significantly lower than that before fracture due to the compaction of the goaf (see Fig. 7(d)). The energy in front of the coal wall was reduced from 210.13 KJ/m^3 to 160.01 KJ/m^3, which was 50.12 KJ/m^3 lower than that before breaking, with a reduction of 23.85%. Under the influence of the breaking impact of TMR, large energy MS events were easily induced in front of the working face.

3.2 Effect of MR thickness on surrounding rock fracture and instability law

3.2.1 Movement of overlying strata

Fig. 8 shows the change curve of subsidence of overlying strata of different thickness of MR before fracture. With the increase of the thickness of the MR, the subsidence of the overlying strata tended to increase. For every 10 m increase of the average MR thickness, the maximum subsidence of the overlying strata increased by 0.048 m. However, the subsidence difference between 80 m thick and 40 m TMR was only 0.191 m, which was mainly due to the relatively small tensile deformation of MR with relatively large bending strength before fracture. Due to its control and support to the overlying strata, the amount of subsidence of the overburden was also small. In addition, the thicker the MR, the wider the subsidence span of the overlying strata (the larger the subsidence range).

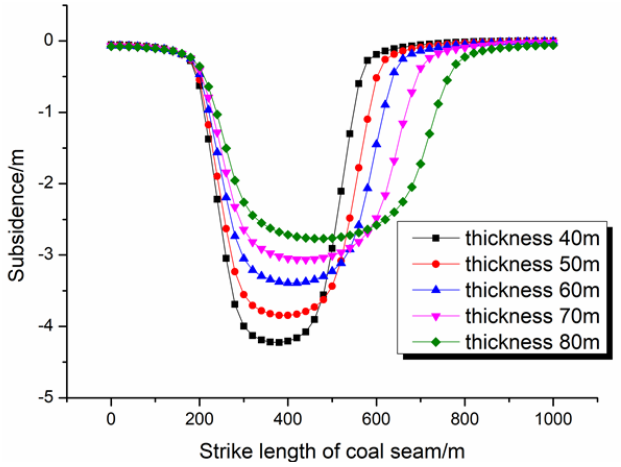

Fig. 9 Subsidence of overlying strata after the breaking of MR with different thickness

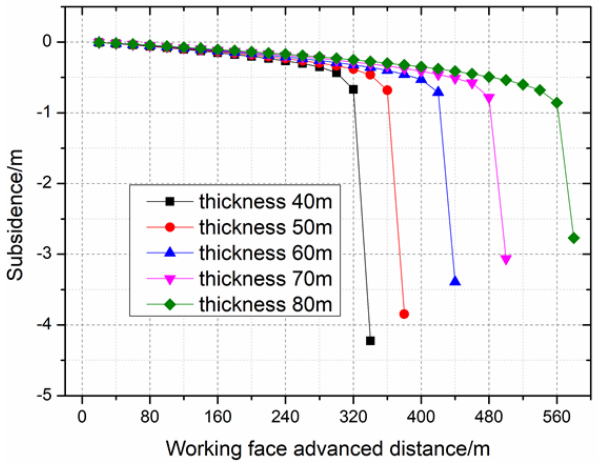

Fig. 10 Variation curve of maximum subsidence of overlying strata before and after initial breakage of MR with different thickness

Table 2 Subsidence of overlying strata before and after breaking of MR with different thickness

Thickness /m	Breaking span /m	Before breaking /m	After breaking /m	Increment /%
40	320	0.668	4.224	532.34
50	360	0.681	3.845	464.61
60	420	0.710	3.390	377.46
70	480	0.781	3.064	292.32
80	560	0.859	2.770	222.47

Fig. 9 shows the subsidence of the overlying strata of MR with different thickness after fracture. With the increase of the thickness of the MR, the subsidence of the overlying strata decreased gradually, and the subsidence of the

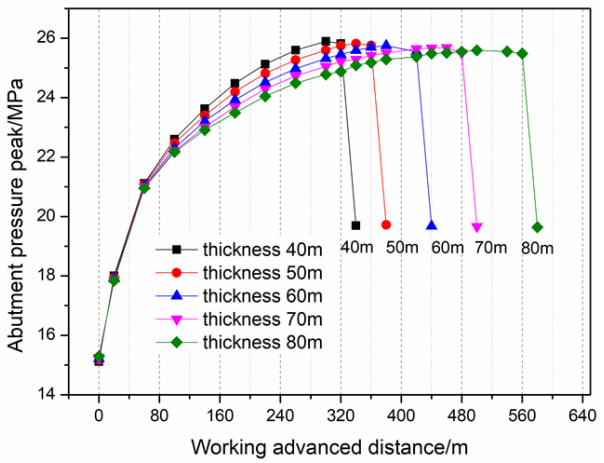

Fig. 11 Peak variation curve of abutment pressure in front of working face under different thickness MR

Table 3 Abutment pressure peak and influence range in front of working face under different thickness MR

Thickness/m		40	50	60	70	80
Maximum	Peak/MPa	25.90	25.82	25.75	25.68	25.59
	Stress Concentration Factor	1.73	1.72	1.72	1.71	1.71
	Influence range/m	205	215	225	240	315
Before breaking	Peak/MPa	25.82	25.76	25.54	25.51	25.48
	Stress Concentration Factor	1.72	1.72	1.70	1.70	1.70
After breaking	Peak/MPa	19.70	19.72	19.68	19.66	19.64
	Stress Concentration Factor	1.31	1.31	1.31	1.31	1.31
Reduction/%		23.70	23.45	22.94	22.93	22.92

*Note: the influence range of abutment pressure is 5% higher than the original rock stress as the boundary

Table 4 Variation law of elastic energy in the middle part of coal seam before and after fracture of different thickness MR

Thickness/m		40	50	60	70	80
Peak value along crossheading/ 10^3KJ/m^3	Before breaking	224.58	226.18	228.17	230.51	231.29
	After breaking	251.33	256.76	260.09	263.24	265.36
	Increment/ %	11.91	13.52	13.99	14.20	14.73
Peak value in front of coal wall/10^3KJ/m^3	Before breaking	212.87	212.63	210.46	210.13	210.01
	After breaking	160.47	160.34	160.24	160.01	159.98
	Reduction /%	24.62	24.59	23.86	23.85	23.82

overlying strata decreased by 0.364 m for every 10 m increase of the average thickness of the MR. The subsidence span of the overlying strata (i.e., the subsidence range) also increased with increasing thickness, but the corresponding basin edge movement deformation value became smaller (subsidence was gentle).

In order to intuitively understand the movement rule of the overlying strata, the maximum subsidence change curve was drawn as shown in Fig. 10. Fig. 10 shows that in the relatively stable stage of TMR, the thickness of MR had little influence on the displacement change of overlying strata, and the subsidence of overlying strata of different thickness of MR kept increasing synchronously. From the beginning of the significant activity stage, with the increase of the thickness of MR, the subsidence speed of the overlying strata gradually decreased, but the breaking span and the maximum subsidence before the breaking increased. The maximum subsidence after breaking was significantly increased compared with that before breaking, but the increasing range was gradually reduced, as shown in Table 2 .

3.2.2 Distribution characteristics of front abutment pressure of working face

Fig. 11 shows the peak variation curve of abutment pressure in front of the working face with different thickness of MR. It shows that the larger the thickness of MR was, the slower the growth rate of abutment pressure in front of the working face was, and the larger the first breaking span was, but the peak value of abutment pressure in front of the working face was smaller, and the influence range was larger; after the break, the reduction range of abutment pressure in front of the working face decreased with the increase of thickness, and the stress concentration coefficient was maintained at about 1.31 (see Table 3).

3.2.3 Energy distribution characteristics

Fig. 12 is the top view of the elastic energy change characteristics in the middle of the coal seam before and after breaking when the thickness of MR was 40 m, 50 m, 60 m, 70 m and 80 m respectively. With the increase of MR thickness, the range of "O" type energy concentration circle before fracture was gradually enlarged, and the range of high energy concentration area around the goaf was gradually increased, but the energy in front of the coal wall and along the crossheading showed the opposite growth trend with the increase of MR thickness (see Table 4). After the fracture, the energy along the crossheading increased, and the thicker the MR, the greater the increase rate. The energy peak in front of the coal wall showed a decreasing trend. As the thickness of the MR increased, the energy reduction rate gradually decreased after breaking. At this time, the coal and rock mass may be destroyed or moved suddenly, thrown to the mined space, forming rock burst (Petrolito 2014, Jiang et al. 2019, Sadoun et al. 2018, Yu *et al*. 2018).

4. Case study

4.1 Outline of 104 mining area in Yangliu Coal Mine

Yangliu Coal Mine is located in Huaibei City, Anhui Province, China, with an area of 60.4 km^2 and recoverable reserves of 140.56 million tons. The mine field is about 9 km long from south to North and about 3-9 km wide from east to west. Mining area 104 is located in the southeast of

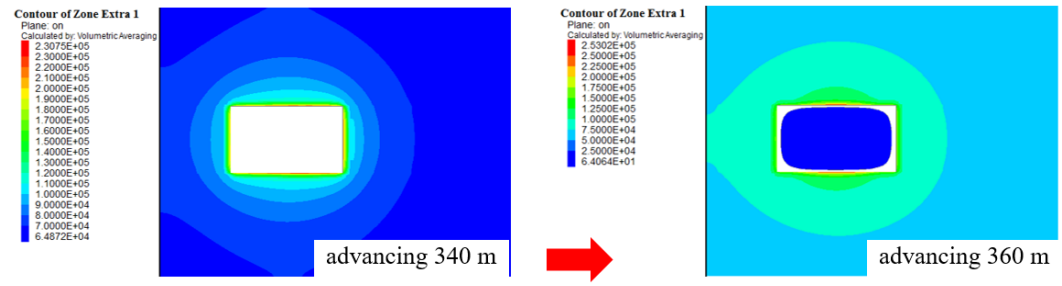

(i) Before breaking (ii) After breaking

(a) Thickness 40 m

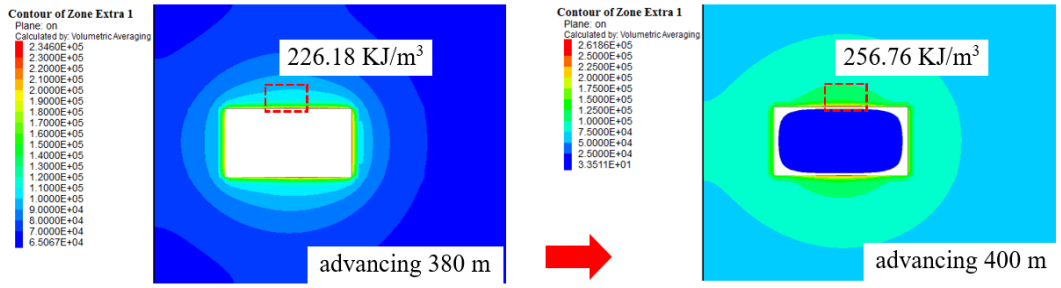

(i) Before breaking (ii) After breaking

(b) Thickness 50 m

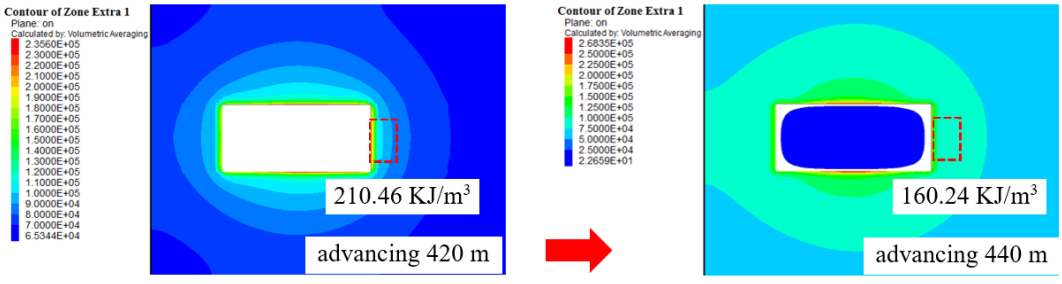

(i) Before breaking (ii) After breaking

(c) Thickness 60 m

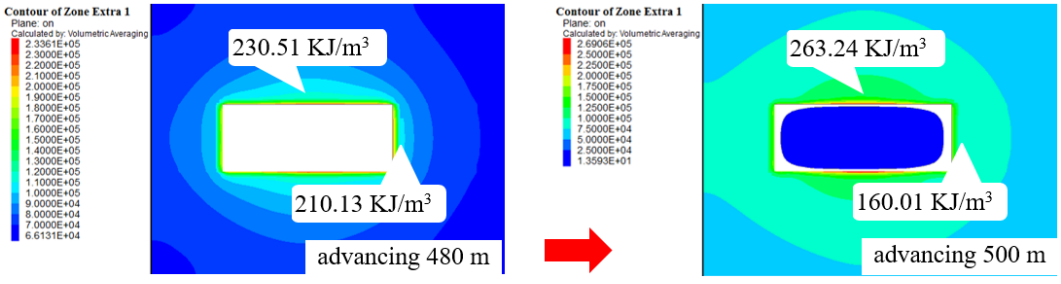

(i) Before breaking (ii) After breaking

(d) Thickness 70 m

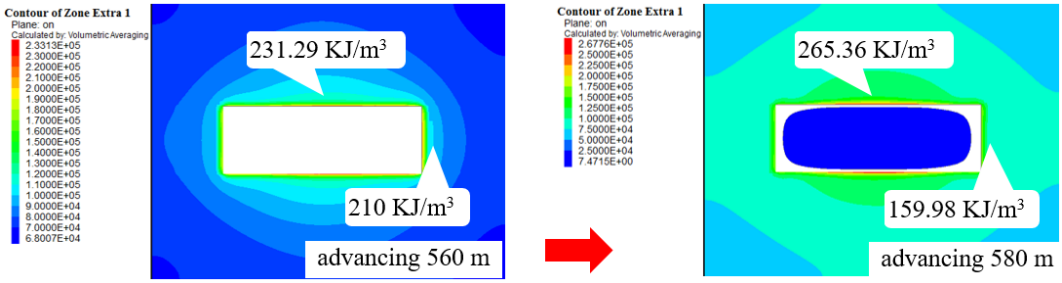

(i) Before breaking (ii) After breaking

(e) Thickness 80 m

Fig. 12 Top view of elastic energy distribution in the middle of coal seam before and after fracture of different thickness MR

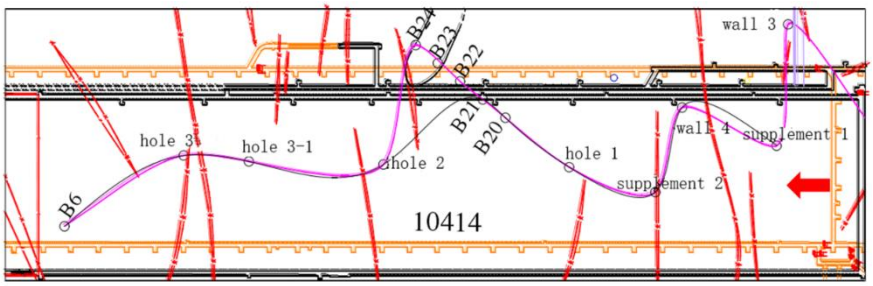

Fig. 13 10414 working surface ground settlement measurement point layout (Zhang *et al.* 2014)

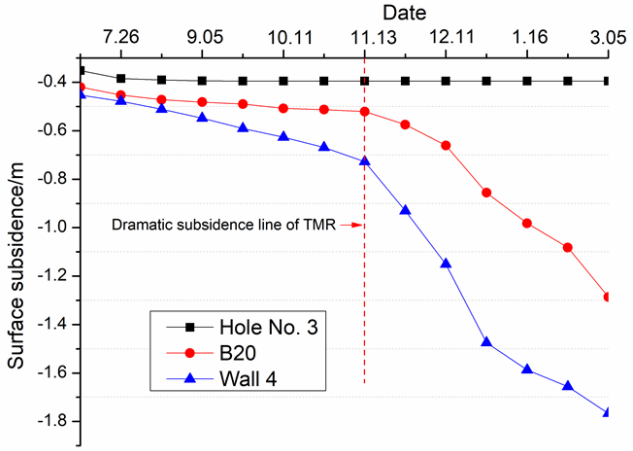

Fig. 14 Dynamic subsidence curve of surface settlement measured points along 10414 striking direction

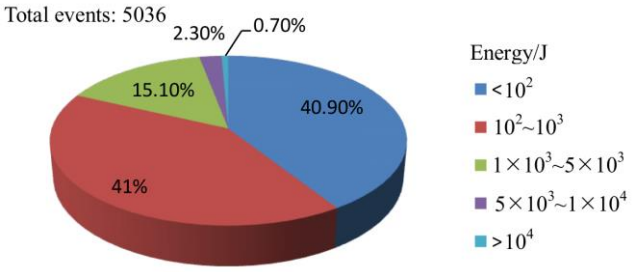

Fig. 15 Piece chart of MS distribution of different energy levels

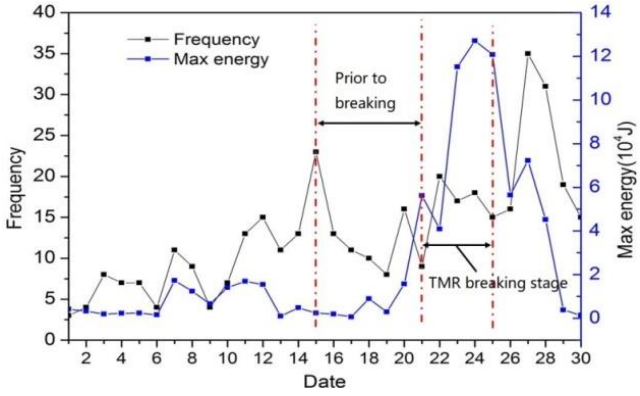

Fig. 16 Maximum released energy and frequency in November (Jiang *et al.* 2019)

the mine, with an area of about 2.12 km^2. 10 coal seam is the main coal seam in 104 mining area, with an average buried depth of 600 m, thickness variation range of 0-7.97 m and an average value of 3.05 m. The roof of coal seam 10 is mostly sandstone and mudstone with a little siltstone, and there is MR with an average thickness of 43.5 m at 116 m above.

4.2 Surface settlement observation

The first mining face 10414 is located in the east wing of mining area 104, with the upper working face 10416 and the lower working face 10412. In order to effectively control the surface subsidence of the working face and ensure safe production, 10 monitoring points were arranged along the strike direction of the 10414 working face, as shown in Fig. 13. Starting from the vicinity of the open-off cutting hole, they are: A36, supplement 1, wall 4, supplement 2, hole 1, B20, hole 2, hole 3-1, hole 3 and hole B6. Extract the displacement settlement values of hole 3, B20 and wall 4, and draw the settlement curve as shown in Fig. 13.

Fig. 14 shows that before November 11, 2011, the TMR was in a relatively stable stage, the surface subsidence of working face 10414 was very small, and the TMR controlled the subsidence movement of the surface (Zhang *et al.* 2014). From November 13, the surface subsidence of B20 and wall 4 measuring points increased significantly, and the subsidence of wall 4 measuring point in the air way position was significantly greater than that of B20 measuring point in the middle of the working face, the maximum subsidence reached 1.8 m, indicating that the TMR in the goaf of 10414 face had a dramatic migration. The breaking of TMR can affect the dynamic subsidence process of the earth's surface, and the breaking of overlying TMR can accelerate the subsidence of the earth's surface.

4.3 MS events and analysis

Microseismic activity is a significant indicator for detecting blast-prone areas. The location of blast-prone areas changes with the progress of mining activities. By recording the waveform, the microseismic monitoring system is extensively adopted to estimate the location of microseisms in coal mines (Domański and Gibowicz 2008, Bischoff *et al.* 2010, Sainoki and Mitri 2014).

10416 is the replacement working face of 10414 working face, on which is the goaf of 10414 working face. According to the real-time MS monitoring data of SOS monitoring system during the stoping period of 10416

working face (Zhang *et al.* 2014), the statistical analysis shows the vibration occurrence from July 12, 2012 to September 30, 2013, as shown in Fig. 15.

As shown in Fig. 15, 5036 microseisms occurred in total in 10416 mining processes, and the MS activities below 10^3 J accounted for 81.9% of the total frequency, indicating that the MS intensity was relatively small, mainly small energy vibration, and the threat to the working face was relatively small. The MS events of more than 10^4 J only accounted for 0.7%, which shows that the integrity of the overlying TMR is good and it can keep stable for a long time. With the advance of working face, once the bed separation reached the limit span of TMR, bending and tensile fracture occurred, and a large amount of energy was released instantly, resulting in a strong earthquake in the mine.

Fig. 16 shows the maximum daily release energy and frequency of 10416 working face in November 2012. The frequency of MS events was generally on the rise from November 1 to 19, but the energy change was relatively stable and at a low level. During this period, the elastic energy accumulated in the coal seam and overburden was easy to release in the form of small vibration, which had little threat to the impact of the working face, but it was easy to induce further fracture of the coal body. With the advance of the working face, the overburden collapse gradually developed to a high level, and the large energy MS events became the main one. According to statistics, there were 6 times of MS energy higher than 5×10^4 J during November 20 to 28, including 3 times of events above 1×10^5 J. The energy reached the maximum on the 24th, and the microseismic activities of different levels frequently occurred. The frequent occurrence of large energy microseisms was caused by the breaking and subsidence of MR. In the process of breaking and subsidence, MR released a large number of elastic energy, which propagated to the surrounding in the form of shock waves. In addition, the gravity potential energy released by the subsidence movement was very easy to induce strong dynamic disasters such as working face impact ground pressure and mine shock. After the MR fracture, the MS energy value showed a downward trend, but the MS frequency remained at a high level. This was due to the dynamic disturbance of the lower strata caused by the fracture settlement of TMR, which further induced small energy microseisms.

5. Conclusions

We have established a 3-D numerical model to simulate the fracture and instability law of mining surrounding rock under different thicknesses of MR conditions. Morever, a case study was conducted to verify the disaster-causing mechanism of our simulated TMR. The main conclusions can be summarized as follows:

• Due to the large bending strength of MR, the subsidence of overlying strata before fracture is less affected by the thickness of MR. After the fracture, the subsidence of the overlying strata increases sharply, and the larger the thickness of the MR, the smaller the subsidence of the overlying strata, but the subsidence span of the overlying strata become wider, and the corresponding displacement deformation value of the basin edge become smaller (the subsidence is gentle).

• The larger the thickness of MR, the slower the growth rate of abutment pressure in front of the working face, and the larger the first breaking span, but the peak value is smaller, and the influence range is larger. The peak value before the breaking decreases slightly. The front abutment pressure decreases rapidly after the breaking and there is a significant mutation. The reduction range of abutment pressure decreases with the increase of thickness, and the stress concentration coefficient is maintained at about 1.31.

• Under the influence of TMR, the energy concentration around the goaf appeares as isoline “O” type energy circle. Increases in thickness increase the peak energy at crossheading and therefore increase breaking impact tendency. Increases in thickness decrease peak energy in front of coal wall, but the range of energy concentration increases.

Acknowledgments

This research was financially supported by the National Natural Science Foundation of China(Grant No.51974172) , China Postdoctoral Science Foundation (2015M572067), Postdoctoral Innovation Project of Shandong Province (152799), Qingdao Postdoctoral Applied Research Project (2015203), Natural Science Foundation of Shandong Province (ZR2019MEE004) and the Shandong University of Science and Technology (SDUST) Research Fund (2018TDJH102).

References

Bischoff, M., Cete, A., Fritschen, R. and Meier, T. (2010), “Coal mining induced seismicity in the Ruhr area, Germany”, *Pure Appl. Geophys*., **167**(1-2), 63-75. http://dx.doi.org/10.1007/s00024-009-0001-8.

Chen, S.J., Yin, D.W., Jiang, N., Wang, F. and Guo, W.J. (2019), “Simulation study on effects of loading rate on uniaxial compression failure of composite rock-coal layer”, *Geomech. Eng*., **17**(4), 333-342. https://doi.org/10.12989/gae.2019.17.4.333.

Dewandel, B., Lachassagne, P., Zaidi, F.K. and Chandra, S. (2011), “A conceptual hydrodynamic model of a geological discontinuity in hard rock aquifers: Example of a quartz reef in granitic terrain in South India”, *J. Hydrol*., **405**(3-4), 474-487. https://doi.org/10.1016/j.jhydrol.2011.05.050.

Dou, L.M., Mu, Z.L., Li, Z.L., Cao, A.Y. and Gong, S.Y. (2014), “Research progress of monitoring, forecasting, and prevention of rockburst in underground coal mining in China”, *Int. J. Min. Sci. Technol*., **1**(3). https://doi.org/10.1007/s40789-014-0044-z.

Domański, B. and Gibowicz, S.J. (2008), “Comparison of source parameters estimated in the frequency and time domains for seismic events at the Rudna copper mine, Poland”, *Acta Geophys*., **56**(2), 324-343. https://doi.org/10.2478/s11600-008-0014-1.

Fu, T.F., Xu, T., Heap, M.J., Meredith, P.G. and Mitchell, T.M. (2020), “Mesoscopic time-dependent behavior of rocks based on three-dimensional discrete element grain-based model”, *Comput. Geotech*., **121C**, 103472. https://doi.org/10.1016/j.compgeo.2020.103472.

Herget, G. (1987), “Stress assumptions for underground

excavations in the canadian shield", *Int. J. Rock Mech. Min. Sci. Geomech. Abstr.*, **24**(1), 95-97. https://doi.org/10.1016/0148-9062(87)91238-1.

Heal, D. (2010), "Observations and analysis of incidences of rockburst damage in underground mines", Ph.D. Dissertation, University of Western Australia, Perth, Australia.

Itasca (2012), *Fast Lagrangian analysis of Continua*, Itasca Consulting Group Inc, Minneapolis, Minnesota, U.S.A.

Jiang, L.S., Wu, Q.S., Wu, Q.L., Wang, P., Xue, Y.C., Kong, P. and Gong, B. (2019), "Fracture failure analysis of hard and thick key layer and its dynamic response characteristics", *Eng. Fail Anal.*, **98**, 118-130. https://doi.org/10.1016/j.engfailanal.2019.01.008.

Jiang, J.Q., Wang P., Wu Q.L and Zhang P.P. (2015), "Evolution laws and prediction of separated stratum space under overlying high-position magmatic rocks", *Chin. J. Geotech. Eng.*, **37**(10), 1769-1779. https://doi.org/10.11779/CJGE201510004.

Keneti, A. and Sainsbury, B.A. (2018), "Characterization of strain-burst rock fragments under a scanning electron microscope - An illustrative study", *Eng. Geol.*, **246**, 12-18. https://doi.org/10.1016/j.enggeo.2018.09.025.

Konicek, P., Soucek, K., Stas, L. and Singh, R. (2013), "Long-hole destress blasting for rockburst control during deep underground coal mining", *Int. J. Rock Mech. Min. Sci.*, **61**, 141-153. https://doi.org/10.1016/j.ijrmms.2013.02.001.

Liu, X.J. and Cheng, Z.B. (2019), "Changes in subsidence-field surface movement in shallow-seam coal mining", *J. S. Afr. I. Min. Metall.*, **119**(2), 201-206. https://doi.org/10.17159/2411-9717/2019/v119n2a12.

Lu, C.P., Liu, Y., Wang, H.Y. and Liu, P.F. (2016), "Microseismic signals of double-layer hard and thick igneous strata separation and fracturing", *Int. J. Coal Geol.*, **160**, 28-41. https://doi.org/10.1016/j.coal.2016.04.011.

Mazaira, A. and Konicek, P. (2015), "Intense rockburst impacts in deep underground construction and their prevention", *Can. Geotech. J.*, **52**(10), 1426-1439. https://doi.org/10.1139/cgj-2014-0359.

Nawrocki, P. (1990), "Rock burst initiation as an instability phenomenon", *Arch. Gorn.*, **35**(1), 115-159.

Naji, A.M., Emad, M.Z., Rehman, H. and Yoo, H. (2019), "Geological and geomechanical heterogeneity in deep hydropower tunnels: A rock burst failure case study", *Tunn. Undergr. Sp. Technol.*, **84**, 507-521. https://doi.org/10.1016/j.tust.2018.11.009.

Petrolito, J. (2014), "Vibration and stability analysis of thick orthotropic plates using hybrid-Trefftz elements", *Appl. Math. Model.*, **38**(24), 5858-5869. https://doi.org/10.1016/j.apm.2014.04.026.

Qian M.G., Miu X.X. and Xu J.L (1996), "Theoretical study of key stratum in ground control", *J. China Coal Sci.*, **21**(03), 2-7. https://doi.org/10.13225/j.cnki.jccs.1996.03.001.

Sadoun, M., Houari, M.S.A., Bakora, A., Tounsi, A., Mahmoud, S.R. and Alwabli, A.S. (2018), "Vibration analysis of thick orthotropic plates using quasi 3D sinusoidal shear deformation theory", *Geomech. Eng.*, **16**(2), 141-150. https://doi.org/10.12989/gae.2018.16.2.141.

Sun, W.B., Xue, Y.C., Li, T.T. and Liu, W.T. (2019a), "Multi-field Coupling of Water Inrush Channel Formation in a Deep Mine with a Buried Fault", *Mine Water Environ.*, **38**(3), 528-535. https://doi.org/10.1007/s10230-019-00616-2.

Sun, W.B., Xue, Y.C., Yin, L.M. and Zhang, J.M. (2019b), "Experimental study on seepage characteristics of large size rock specimens under three-dimensional stress", *Geomech. Eng.*, **18**(6), 567-574. https://doi.org/10.12989/gae.2019.18.6.567.

Swift, G. (2014), "Relationship between joint movement and mining subsidence", *Bull. Eng. Geol. Environ.*, **73**(1), 163-176. https://doi.org/10.1007/s10064-013-0539-7.

Sainoki, A. and Mitri, H.S. (2014), "Methodology for the interpretation of fault-slip seismicity in a weak shear zone", *J. Appl. Geophys.*, **110**(Nov), 126-134. https://doi.org/10.1016/j.jappgeo.2014.09.007.

Sun, W.B. and Xue, Y.C. (2019), "An improved fuzzy comprehensive evaluation system and application for risk assessment of floor water inrush in deep mining", *Geotech. Geol. Eng.*, **37**(3), 1135-1145. https://doi.org/10.1007/s10706-018-0673-x.

Tadisetty, S., Matsui, K., Shimada, H. and Gupta, R.N. (2006), "Real time analysis and forecasting of strata caving behaviour during longwall operations", *Rock Mech. Rock Eng.*, **39**(4), 383-393. https://doi.org/10.1007/s00603-005-0077-0.

Wang, W., Cheng, Y.P., Wang, H.F., Liu, H.Y., Wang, L., Li, W. and Jiang, J.Y. (2015), "Fracture failure analysis of hard-thick sandstone roof and its controlling effect on gas emission in underground ultra-thick coal extraction", *Eng. Fail. Anal.*, **54**, 150-162. https://doi.org/10.1016/j.engfailanal.2015.04.016.

Wu, Q.L., Wu, Q.S., Xue, Y.C., Kong, P. and Gong, B. (2018), "Analysis of overlying strata movement and disaster-causing effects of coal mining face under the action of hard thick magmatic rock", *Processes*, **6**(9), https://doi.org/10.3390/pr6090150.

Wang L., Cheng Y.P., Xu, C., An, F.H., Jin, K. and Zhang, X.L. (2013), "The controlling effect of thick-hard igneousrock on pressure relief gas drainage and dynamic disasters in outburst coal seams", *Nat. Hazards,* **66**(2), 1221-1241. https://doi.org/10.1007/s11069-012-0547-0.

Xu, C., Fu, Q., Cui, X.Y., Wang, K., Zhao, Y.X. and Cai, Y.B. (2019), "Apparent-depth effects of the dynamic failure of thick hard rock strata on the underlying coal mass during underground mining", *Rock Mech. Rock Eng.*, **52**(5), 1565-1576. https://doi.org/10.1007/s00603-018-1662-3.

Yu, X.Y., Xu, T., Heap, M., Zhou, G.L. and Baud, P. (2018) "Numerical approach to creep of rock based on the numerical manifold method", *Int. J. Geomech.*, **18**(11), 04018153. https://doi.org/10.1061/(ASCE)GM.1943-5622.0001286.

Zhang P.P., Jiang L.S., Liu X.F., Zhang Z.L. and Liu X. (2017), "Mining-induced overlying strata structure evolution characteristics and disaster-triggering under high level hard thick strata", *J. Min. Saf. Eng.*, **34**(5), 852-860. https://doi.org/10.13545/j.cnki.jmse.2017.05.005.

Zhang R.B. (2014), "Fracturing migration rules of double thick-hard igneous in Yangliu Coal Mine", M.A. Dissertation, China Mining University, Beijing, China

Zhou F., Sun W.B., Shao J.L., Kong L.J. and Geng X.Y. (2020a), "Experimental study on nano silica modified cement base grouting reinforcement materials", *Geomech. Eng.*, **20**(1), 67-73. https://doi.org/10.12989/gae.2019.18.6.567.

Zhou, G.L., Xu, T., Heap, M.J., Meredith, P.G., Mitchell, T.M., Sesnic, A.S.Y. and Yuan, Y. (2020b), "A three-dimensional numerical meso-approach to modeling time- independent deformation and fracturing of brittle rocks", *Comput. Geotech.*, **117**, 103274. https://doi.org/10.1016/j.compgeo.2019.103274.

Zhao, J.H., Yin, L.M. and Guo, W.J. (2018), "Stress-seepage coupling of cataclastic rock masses based on digital image technologies", *Rock Mech. Rock Eng.*, **51**(8), 2355-2372. https://doi.org/10.1007/s00603-018-1474-5.

Zhao, J.H., Zhang, X.G., Jiang, N., Yin, L.M. and Guo, W.J. (2020), "Porosity zoning characteristics of fault floor under fluid-solid coupling", *Bull. Eng. Geol. Environ.* https://doi.org/10.1007/s10064-019-01701-0.

GC